EFFECT OF DIVERTOR PLASMA CONFIGURATION ON CORE AND DIVERTOR PLASMA PERFORMANCE IN THE DIII–D TOKAMAK

M.E. FENSTERMACHER,[1] T.W. PETRIE,[2] J.G. WATKINS,[3] M.A. MAHDAVI,[2] T.H. OSBORNE,[2] M.R. WADE,[4] N.S. WOLF,[1] T.N. CARLSTROM,[2] R.J. GROEBNER,[2] A.W. HYATT,[2] C.J. LASNIER,[1] R.J. LA HAYE,[2] A.W. LEONARD,[2] G.D. PORTER,[1] AND THE DIII–D TEAM

[1]*Lawrence Livermore National Laboratory, P.O. Box 808, Livermore, California, USA*

[2]*General Atomics, P.O. Box 85608, San Diego, California 92186-5608, USA*

[3]*Sandia National Laboratories, P.O. Box 5800, Albuquerque, New Mexico*

[4]*Oak Ridge National Laboratory, Oak Ridge, Tennessee, USA*

Abstract — Systematic configuration variation experiments were done using ELMing H–mode plasmas in DIII–D. The response of core, pedestal, scrape-off-layer (SOL), and divertor plasma performance was examined versus *triangularity*, δ, *up/down magnetic balance*, DR_{sep}, and secondary *divertor volume*. Results indicate that for high-δ operation an unbalanced DN shape has some advantages over a single-null shape for future high power tokamak operation. The effects of closing the divertor region with baffling on the divertor pumping (low n_e) and detachment (high n_e) were studied using matched lower and upper single-null plasmas with different baffling in a single DIII–D campaign. Unpumped plasmas with divertor baffling exhibit reduced core fueling rate and also reduced core carbon content compared with unbaffled configurations. In attached plasmas at low to moderate density with divertor baffling and pumping, and ion ∇B drift toward the divertor, the exhaust rate of either the pump in the SOL or in the private flux region is correlated with the proximity of the separatrix strikepoint to the pump entrance. The pumping is less sensitive to strikepoint position in detached divertor operation. Finally, optimized pumping geometry with baffling produces a low core plasma density that is desirable for non-inductive current drive scenarios.

1. INTRODUCTION

The optimization of the tokamak as a fusion energy source [1] is focussing more and more on operation of the plasma with a high triangularity shape and this brings with it implications for divertor design and operation. Tokamak plasmas with a high triangularity shape have higher normalized core energy confinement and beta limit in ELMy H–mode than those with lower triangularity [2,3]. In addition, for fixed safety factor, the total plasma current can be higher in a high triangularity shape. Combining all of these factors leads to significantly higher fusion power density in high triangularity plasmas. However, high triangularity shapes have different requirements on the divertor operation and design than low triangularity shapes. For coil designs with the poloidal field coils outside the toroidal field coils, high triangularity tends to lead to nearly balanced double-null plasma operation. This implies that a significant fraction of the volume inside the TF coils will be used by the second divertor thereby reducing the volume available to the core plasma. The trade-offs between single-null (SN) versus double-null (DN) divertor operation and between plasma volume used for the core veersus divertor plasma must be understood quantitatively before optimized tokamak designs can be generated.

This paper describes experiments [4–13] that have increased our understanding of the complex coupling of core and divertor plasma performance to the divertor plasma configuration. Systematic studies were done using Type-I ELMing [14] H–mode plasmas in which the independent variables were the shape of the core plasma, the divertor plasma, and the divertor structures [4–10]. These studies complement the shape variation work done elsewhere in the world (see review in [14] and references therein). The discharge scenarios are briefly described in Section 2. The effect of variations in the core and divertor shape on attached and detached divertor operation are given in Section 3. Then Section 4 describes the effects of changes in divertor baffling configuration on divertor pumping in attached plasmas [11,12] and on detachment

characteristics in high density plasmas [13]. A summary and conclusions are presented in Section 5.

2. DISCHARGE DESCRIPTIONS

Systematic studies of the effect of shape variation in the plasma and the divertor structures for both low and high density regimes were done by varying the shape from one discharge to the next and varying the density within the discharge using gas injection. The diversity of core and divertor plasma shape variations is shown schematically in Fig. 1. Shape variation studies were typically done by varying the shape from one discharge to the next and varying the density within the discharge using gas injection. As an example, the discharge evolution from one of the secondary X–point height variation studies discharge evolution is shown in Fig. 2. This example shows the typical discharge sequence in which the current flattop and desired plasma shape were established first and then followed by neutral beam injection to produce an

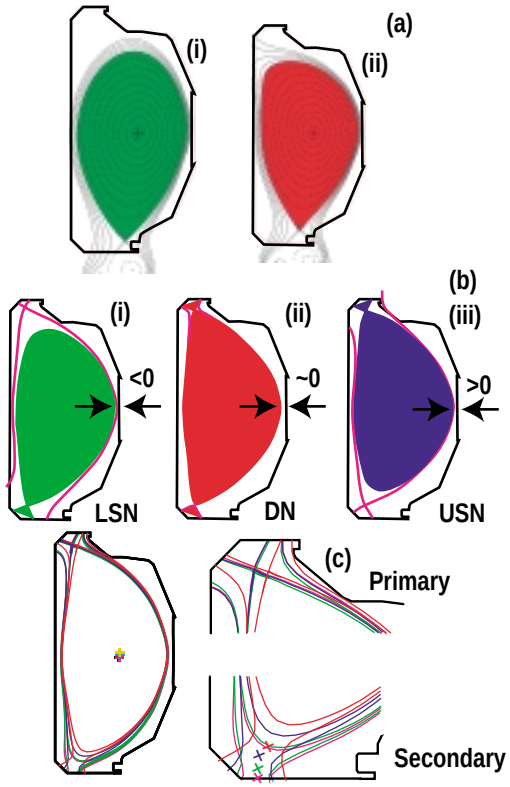

FIG. 1. Plasma shapes used in these experiments. (a) Shapes from triangularity variations: (ai) low triangularity and (aii) high triangularity, (b) from up/down magnetic balance studies: (bi) LSN $dR_{sep} < 0$, (bii) DN $dR_{sep} = 0$, (biii) USN, $dR_{sep} > 0$, and (c) from secondary X–point height variations (expanded divertor views shown).

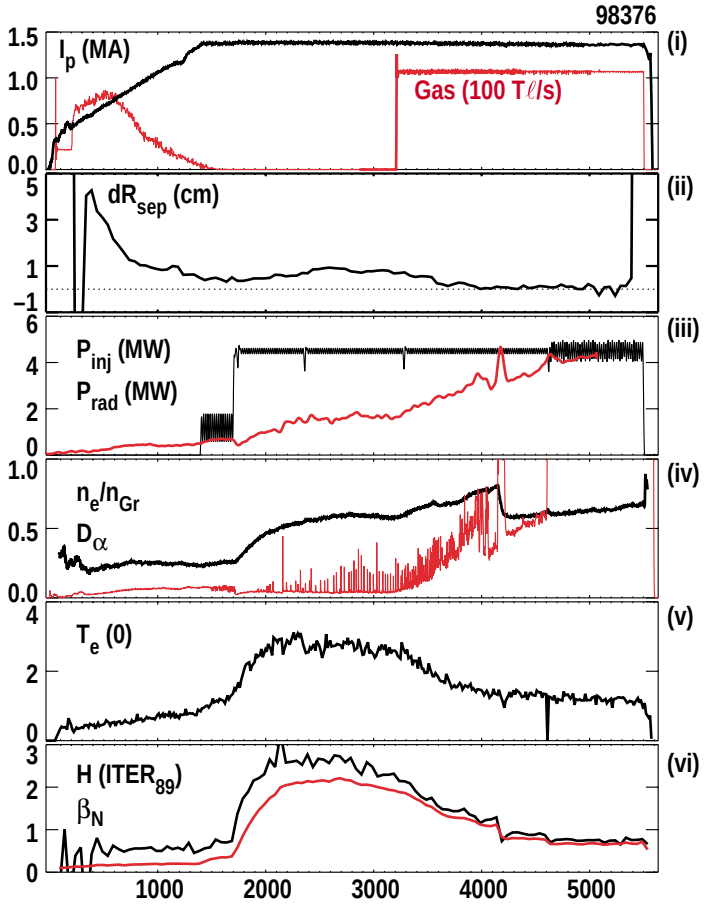

FIG. 2. Evolution of discharge parameters used in the experiments with constant plasma shape and gas injection to produce a density ramp. Parameters are: (i) plasma current, I_p (MA), gas injection (100 Tl/s), (ii) dR_{sep} (cm), (iii) injected neutral beam power, P_{inj} and total radiated power, P_{rad} (MW), (iv) line-averaged density normalized to Greenwald density and D_α emission (v) central electron temperature, $T_e(0)$ (keV) and (vi) energy confinement normalized to ITER89 L-scaling, H(ITER89L) and normalized beta, $\beta_N = \beta/(I_p/aB_T)$.

ELMing H–mode and gas injection to raise the density to the H-L back transition density limit. A limited number of discharges with constant input conditions and shape variation within the discharge were also done [7]. H–mode plasmas with large Type-I ELMs [15] were used in these studies. Similar studies [16] using VH–mode plasmas [17] were done previously. Typical discharge parameters (and the ranges used in some of the studies) were: plasma current, I_p = 1.4 (0.8–2.0) MA, toroidal field, B_T = 2.0 (1.4–2.1) T, major radius, R_0 = 1.75 m, minor radius, a = 0.6 m, elongation, κ = 2.0 (1.7–2.2), injected neutral beam power, P_{inj} = 5 (2–7) MW, and safety factor at 95% flux, q_{95} = 4.5 (2.25–10).

3. EFFECT OF CHANGES IN CORE AND DIVERTOR PLASMA SHAPE

The choice of the shape for the core and divertor plasmas is made very early in the design of any future tokamak and it can have significant implications for plasma performance. To obtain more complete understanding of these effects, systematic shape variation experiments were done. The response of core, pedestal, scrape-off-layer (SOL), and divertor plasma performance was examined versus triangularity, δ, up/down magnetic balance, parameter dR_{sep}, and secondary divertor X–point height, parameter Z_x^s (Fig. 1). Here dR_{sep} is the midplane radial distance between the upper and lower divertor separatrices. The primary divertor separatrix is the boundary of the closed flux surfaces of the core including an X–point; the secondary divertor separatrix maps from a second X–point to a flux surface that is radially outboard of the primary at the midplane. Z_x^s is the height of the secondary divertor X–point and is a measure of the volume occupied by the secondary divertor. The focus of the experiments was to determine if: (1) increased triangularity improved performance, (2) nearly balanced double-null (DN) shapes had advantages over single-null (SN) shapes and (3) the minimum volume required for the secondary divertor (that will likely appear inside the vacuum vessel for future high triangularity designs), could be predicted.

3.1. Triangularity

The data from the equilibrium shape studies showed that for attached divertor operation a high-δ divertor configuration increases the energy in the H–mode pedestal for a given input power and therefore the global energy confinement of the core plasma [2,3,5]. The pedestal energy increase was due to an increase in the pedestal pressure gradient near the edge of the plasma. The width of the edge pedestal remained unchanged with triangularity variations [5].

For high density operation, increasing triangularity does not produce as much improvement in energy confinement as in lower density attached plasmas. The pedestal pressure, p^{ped}, in the higher triangularity plasma is higher than for the low triangularity

shape at low density. When the line averaged density, n_e, was increased to $n_e \geq 0.7\ n_{Gr}$ the pedestal pressure began to decrease with increasing density. Here n_{Gr} is the Greenwald density limit [17] given by $n_{Gr} = I_p\ (MA)/\pi\ a^2(m)$ where a is the plasma minor radius. Once the reduction in p^{ped} began it was observed to decay at a rate described by $\partial p^{ped}/\partial n \propto \eta^{-0.5}$, where η is the pedestal resistivity [5]. This scaling was independent of δ. Therefore, since p^{ped} and the pedestal temperature, T^{ped}, are higher in the higher δ shape for the density at which p^{ped} begins to decrease, the decay of p^{ped} with increasing density was more rapid than in the lower δ case. This leads to the weak dependence of pedestal pressure on δ at high $n_e/n_{Gr} \sim 1$. However, both the change in pedestal pressure and the response of the density profile play a role in setting the energy confinement. The low δ discharges at high density with divertor pumping showed central density peaking leading to recovery of good confinement [5,9]. A limited number of low δ discharges with central density peaking and no divertor pumping were also obtained [9].

ELMs with a fixed fraction of the pedestal energy given by the scaling $\Delta E_{ELM} = 0.36\ W^{ped}$ [18] were produced at low to moderate density for both low and high triangularity, however at high density with active pumping of the private flux region the fraction of the pedestal energy in the ELM was lower [20]. The ELMs at the lower densities perturbed both the density and temperature in the pedestal region. At high density with active pumping, the smaller rapid ELMs perturbed only the pedestal density; the pedestal temperature remained unchanged during the ELMs. There were indications in the shaping experiments that the minimum density at which the ELMs with low pedestal energy fraction began was somewhat higher in the high δ shape; more detailed experiments are required to confirm this observation.

3.2. Up/Down Magnetic Balance

Results from scans of the up/down magnetic balance of the equilibrium indicate that for high-δ operation an unbalanced DN shape has some advantages over a single-null shape for future high power tokamak operation [4,6–8,10]. In principle for example,

balanced double-null operation could improve the performance of the divertor by sharing the peak heat load in the four divertor target regions. However, the disadvantage of DN shapes is that present design concepts use more of the volume inside the toroidal field coils for divertor plasma and less for the burning core plasma that SN shapes. These and other trade-offs between DN and SN operation are described below. All of the plasmas in this magnetic balance study had the $B \times \nabla|B|$ drift for ions (hereafter referred to as the ion ∇B drift) toward the lower divertor.

3.3. Moderate Density Attached Plasmas

A nearly magnetically balanced double-null (DN) shape with two divertors is effective for sharing the peak heat flux in the outer divertor target regions. For attached plasmas the shift of the peak in the outer heat flux from one divertor to the other occurs for a small variation in the magnetic balance parameter, dR_{sep} near a balanced double-null [4,7,8,10]. The characteristic width in dR_{sep} of a hyperbolic tangent fit to the peak heat flux balance as a function of dR_{sep} was comparable to radial scale width of the parallel heat flux in the SOL at the outer midplane. This indicated that divertor processes were not dominating the scaling. Peak heat flux to the inner divertor targets was significantly smaller than to the outer targets (see discussion in Section 5).

The important physics for determining the dependence of the heat flux balance on magnetic balance in attached plasmas was electron conduction in the SOL [4,8]. It was found that the measured heat flux width could be calculated to within a factor of 2 from a simple conduction model using the measured density and temperature radial SOL widths at the midplane. Hence, for future nearly balanced DN tokamak designs the variation of the heat flux balance between the two divertors in attached divertor operation should be predictable if scalings for the radial SOL widths of density and temperature are available.

Both up/down and in/out asymmetries of the peak heat flux to the divertor legs were observed [8,13]. The upper versus lower outer leg peak heat fluxes were balanced when dR_{sep} was unbalanced 0.3 cm away from the direction of the ion ∇B drift. For ion ∇B

drift into the lower divertor the peak heat flux was higher in the lower outer divertor than the upper outer divertor at magnetic balance, $dR_{sep} = 0$. The peak outer heat flux was always higher than the peak inner heat flux. However, this asymmetry was a factor of 2 larger in the lower divertor (ion ∇B drift direction) than in the upper divertor [8].

Measurements of the dependence of peak particle flux balance on magnetic balance indicated that divertor recycling effects were playing a significant role [4,8,11]. The peak particle flux balance was less sensitive to magnetic balance than was the peak heat flux. In this case the recycling physics in the divertor determines the particle flux profile in the divertor and the width of the shift in dR_{sep} required to shift the peak particle flux from one divertor to the other could not be predicted from simple scaling arguments involving midplane characteristic widths.

Poloidal circulation of particles, due to E×B drift effects, from one divertor leg to the other through the private flux region and from one divertor to the other through the DN SOL may play an important role in up/down asymmetries and in/out asymmetries between the divertor legs [8]. Theoretical work [21] has shown that several “classical” particle drifts [21] may play key roles in driving the observed up/down and in/out divertor asymmetries. The E×B particle drift is one candidate that seems to qualitatively fit the measurements from these studies. The radial electric field that results from the temperature gradient across the separatrix from the divertor leg SOL to the private flux region is always directed into the PF region (Fig. 3). For the divertor in the ion ∇B drift direction (the lower divertor in these studies) the E×B circulation enhances the density near the inner divertor leg (reduces the temperature) and reduces the density (increases the temperature) in the outer leg. In the divertor away from the ion ∇B drift direction (upper divertor) the E×B circulation through the private flux region reduces the inner divertor density (increases the temperature) and increase the outer divertor density (reduces the temperature).

Three observations from the dR_{sep} studies are qualitatively consistent with this model of E×B drift circulation: 1) up/down asymmetries of heat and particle flux, 2) in/out asymmetries and 3) asymmetries in the H-L back transition density [8]. First,

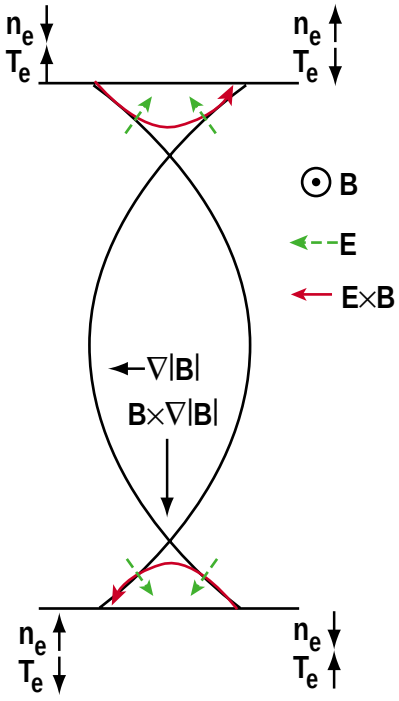

FIG. 3. Schematic of poloidal flows resulting from E×B poloidal drifts for the case with ion ∇B drift toward the lower divertor.

in attached, balanced DN plasmas the data shows that the peak heat flux is unbalanced toward the outer leg of the ion ∇B divertor (lower divertor). The particle flux is unbalanced toward the outer leg of the opposite divertor (upper divertor). Since the heat transport in the SOL of the attached plasmas is dominated by conduction, the higher temperature (lower density) of the outer leg of the lower divertor would be expected to have higher heat conduction than the upper outer leg. This is consistent with the higher heat flux observed on the lower outer target in DN operation. The same E×B circulation that is expected to produce this effect is also expected to produce more particle flux at the upper outer target compared with the lower outer target as observed. Second, the in/out asymmetry of the divertor heat flux was sensitive to the magnetic balance and is largest for the lower divertor in balanced DN shapes. Here the E×B poloidal circulation increases the heat conduction to the lower outer divertor and reduces the conduction to the lower inner divertor. In the upper divertor the E×B circulation has the opposite effect and tends to reduce the in/out asymmetry. Finally, at the highest densities the data show that the density at which the plasma made the transition from H– to L–mode is significantly lower (20%) when the magnetic balance is shifted away from the lower

divertor. One hypothesis under investigation is that at high density the divertor legs are detached and the ionization front is up in the SOL near the X–point in both the divertor legs. The H-L back transition occurs when this ionization front collapses into the core plasma near the X–point [22]. Since, at a given core density, the E×B circulation model predicts that the upper outer divertor leg is at a higher density and lower temperature than the lower outer divertor, then as the core density is increased, the ionization front in the unbalanced DN shape that is shifted towards the upper divertor is expected to collapse at a lower core density than for shapes shifted towards the lower divertor. Modeling of these effects for the data from these stuides is in progress [23].

3.4. High density detached plasmas

In high density plasmas the sensitivity of both the outer leg heat flux and particle flux balance to magnetic balance was quite low indicating that divertor effects were dominant [4,7,8]. Here the outer leg of the divertor was detached and the magnitude of the peak heat fluxes were factors of 3–5 less than in the attached cases. Local ionization and recombination physics in the outer legs determined both the degree of detachment there and the profiles of the heat flux reaching the targets, largely independent of magnetic balance variations.

3.5. ELMs

The shift of the ELM heat flux with dR_{sep} variation was much more gradual than the shift of the time averaged heat flux, consistent with the observed broader deposition of the ELM energy in the SOL [23,7]. For the ELMs in moderate density attached plasmas the energy density profiles at the targets were up to 5 times broader during an ELM than between ELMs. Here the relative insensitivity of ELM energy flux sharing to dR_{sep} is not due to divertor effects but is simply due to the broad deposition of ELM energy in the SOL.

Evidence of ELM activity on Langmuir probes mounted in the target plates disappeared at the inner separatrix strikepoints when the configuration was shifted from an unbalanced to a balanced DN shape; this supports the model that ELM energy is

released from the core plasma into the SOL on the low field side [25]. Discharges with dR_{sep} sweeps from unbalanced DN shapes, $dR_{sep} = \pm 2$, to balanced DN configurations, $dR_{sep} = 0$, showed that the amplitude of the fluctuations in ion saturation current, j_{sat}, from the available probes mounted in the target plates at the inner strikepoints in the upper divertor, was significantly reduced as the balanced DN configuration was approached. The j_{sat} fluctuations near the outer strikepoints did not vary much during these dR_{sep} sweeps. These observations are inconsistent with uniform deposition of ELM energy into the SOL and they point strongly to a model in which the ELM energy is preferentially deposited into the SOL around the outer midplane.

3.6. Secondary Divertor X–point Height

To optimize future tokamak designs with a nearly DN shape the core plasma volume must be maximized and the divertor volume minimized. For unbalanced DN shapes the primary divertor would be designed to handle the majority of the heat load and particle exhaust requirements. Optimization would then seek to minimize the volume of the secondary divertor consistent with good core performance.

The presence of a second X–point in unbalanced DN shapes does not degrade the plasma performance if the secondary X–point is sufficiently far inside the vacuum vessel [6,7]. Systematic reduction in the height of the secondary X–point while holding other shape parameters constant showed that the peak heat flux to the secondary divertor could be reduced due to the increase in flux expansion near the targets until the high recycling character of the secondary divertor was lost at very low X–point height. This occurred roughly when the mean free path of the recycling neutrals in the secondary divertor became comparable to the X–point height and the neutrals were no longer ionized in the secondary divertor. Loss of the high recycling character of the secondary divertor provides a criterion for the minimum secondary divertor volume in the optimization of the design. However, core fueling rate increased and the density at the H-L back transition decreased as the secondary X–point height was reduced even before loss of high recycling character of the secondary divertor. This continuous

degradation of performance with X–point height reduction would need to be considered in the design optimization against the advantages of increasing core plasma volume and fusion power.

4. EFFECT OF CHANGES IN DIVERTOR SHAPE AND BAFFLING

To examine the effect of divertor shape and mechanical baffling, systematic studies of single-null ELMing H–mode plasmas were done using nearly identical shaped plasmas and two different divertors in DIII–D. Comparisons of high triangularity configurations without divertor pumping were done in which the upper divertor had substantial baffling of the outer divertor leg and the private flux region [closed divertor, Fig. 4(a)] and the lower, identically shaped divertor plasma had no baffling[(open divertor, Fig. 4(b)]. The ion ∇B drift was directed into the divertor for each of these cases. The effect of the baffling was significant on several figures-of-merit as described below. The pumping efficiency of the baffled configuration and the effect of inner versus outer leg pumping in SN plasmas were also examined with the ion ∇B drift towards the

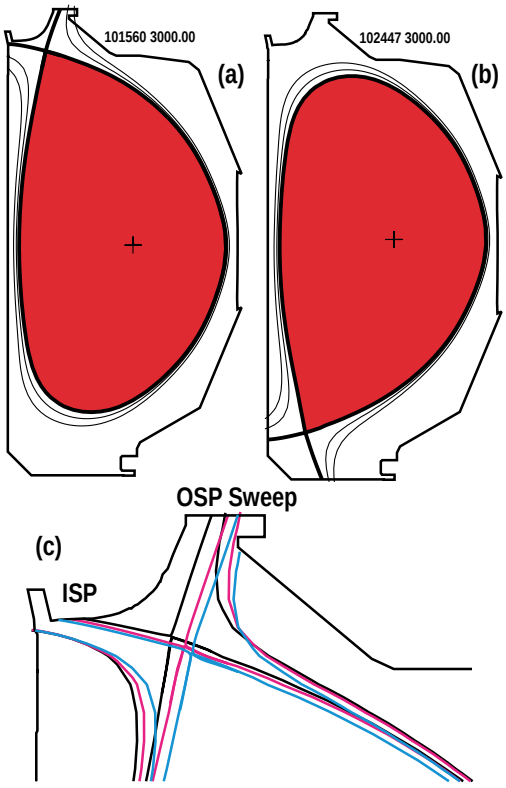

FIG. 4. Plasma and divertor geometries used for the comparisons of open (lower) versus closed (upper) divertor baffling and upper inner versus outer divertor pumping.

baffled, upper divertor. Experiments in DN plasmas investigated the effect of magnetic balance dR_{sep} on the inner and outer leg pumping. Finally, comparisons of low triangularity versus high triangularity lower divertors with minimal baffling (open divertor) showed that the geometry of the inner divertor leg can have a significant effect on divertor performance.

4.1. Detachment

The comparison of a closed divertor (with baffling) and an open divertor (without baffling) in high n_e plasmas without pumping was done by generating identical high triangularity plasmas with I_p = 1.37 MA, κ = 0.74, $|B_T|$ = 2 T, and q_{95} = 4.1 using USN and LSN configurations. In each case the ion ∇B drift was into the divertor so that the H–mode power threshold and the density at the H-L back transition would be expected to be the same except for any dependence on the baffling geometry. Unpumped, high density operation, n_e = 0.6–0.8 n_{Gr}, was compared and matched plasmas with a range of injected power, P_{nb} = 3–7.5 MW were produced.

The comparison of plasma performance in the closed versus open divertor configurations at high density showed that the core carbon concentration and core deuterium fueling rate were measurably less in the closed compared with the open configuration but other figures-of-merit were not affected by the baffling [10,13]. The core carbon concentration was 15%–30% lower with the closed divertor configuration compared with the open divertor for well matched plasma operating conditions including the same core density and injected power. Separate UEDGE modeling of cases with the outer divertor leg baffle alone and with the private flux baffle alone showed that each contributes to reduction of carbon escape from the divertor and less carbon fueling of the core [13,26]. Other factors may also affect carbon content, for example changes in the locations of carbon sources in the open versus closed cases; attempts to model these effects are in progress. The deuterium fueling of the core was 15%–20% lower in the closed configuration. Here modeling showed [13,30] that the divertor baffling did increase the local divertor recycling and density near the target

plates as expected. Also as expected the baffling reduced the escape probability of deuterium from the divertor. The relative reduction in escape probability was larger than the increase in density in the divertor and so the net core fueling (proportional to the product of these factors) decreased in the baffled case. The poloidal profile of the core fueling in the simulations showed a maximum in the inner SOL near the X–point.

The core and edge pedestal densities at outer divertor detachment, and the density at the H– to L–mode transition were similar in the high triangularity open and closed configurations [13]. In this case plasmas with P_{nb} = 3, 5 and 7.5 MW were compared. The pedestal density at detachment onset was 60%–70% higher than the separatrix density at detachment and both increased slightly with injected power (10% increase for a 2× increase in P_{nb}). However, there was no difference outside the error bars in either of these densities between the open and closed configurations. In fact, discharges with the same evolution of macroscopic parameters (injected power, gas puff rate, core density, pedestal density, pedestal temperature and total stored energy) could be made with either the open or closed divertor configurations.

Comparison of high triangularity versus low triangularity open divertors showed that the evolution to detachment with gas injection was sensitive to triangularity. In the low triangularity case partially detached conditions were obtained with normalized energy confinement comparable to the attached case [27]. At high triangularity, as the gas was injected, the initial response of the plasma was that the pedestal temperature decreased without a corresponding increase in pedestal density [13]. This produced a reduction in core energy content and normalized confinement consistent with stiff core temperature profiles. Pedestal density increased with continued gas injection and a gradual evolution of the divertor to detached conditions was observed.

The 2-D profiles of carbon emission in both the open and the closed divertors at high triangularity evolved much more slowly with gas injection from attached to detached profiles than in the low triangularity open divertor. This was an example of the difference in the detachment behavior as a function of divertor shape that was not a function of divertor baffling. Previous studies [28] in low triangularity shapes without

divertor baffling showed that CIII visible emission in attached divertor plasmas is characterized by distributed radiation in the inner SOL near the X–point and along the outer divertor leg to near the outer strikepoint. The change in CIII profile when the outer leg detaches is that the radiation becomes highly localized in the outer SOL near the X–point The evolutions of the CIII visible emission profiles from both the closed (upper) and open (lower) divertors in nearly identically matched single-null plasmas at high triangularity are shown in Fig. 5. The basic characteristic of the change when the divertor detaches is consistent with the previous observations for low triangularity divertor shapes [28]. However, the time scale over which the transition of the CIII profiles, from the start of the evolution after gas injection to detachment, occurs is much longer in the high triangularity cases than previously observed in the lower δ case [29]. In both the open and baffled divertors at high triangularity the time from initiation of the transition after gas injection to the localized CIII profile near the X–point is on the order of two seconds. A comparable discharge with a low triangularity open divertor (Fig. 6) shows that this same transition of the profiles occurs in approximately 300 ms. This is the typical time for these transitions in low triangularity divertors over a range of injected powers and gas puff rates.

Detailed time dependent modeling with a complete carbon model and particle drifts will be required to explain the differences in detachment evolution. In addition to differences in the evolution of the carbon emission, floor probe and other diagnostic data indicated that in the high triangularity cases the inner divertor leg detached at the same time at the outer leg. In low δ open configurations the inner leg always detaches first followed by the outer leg. Contributing factors that might keep the inner leg attached during gas injection in the high δ case include the reduced flux expansion at the inner target and shorter inner leg connection length in these plasmas compared with the low δ cases. However, the fact that the observation is similar in the open and closed divertors may point toward the higher relative importance of recycling and carbon sources outside the divertor in the high δ compared with the low δ cases.

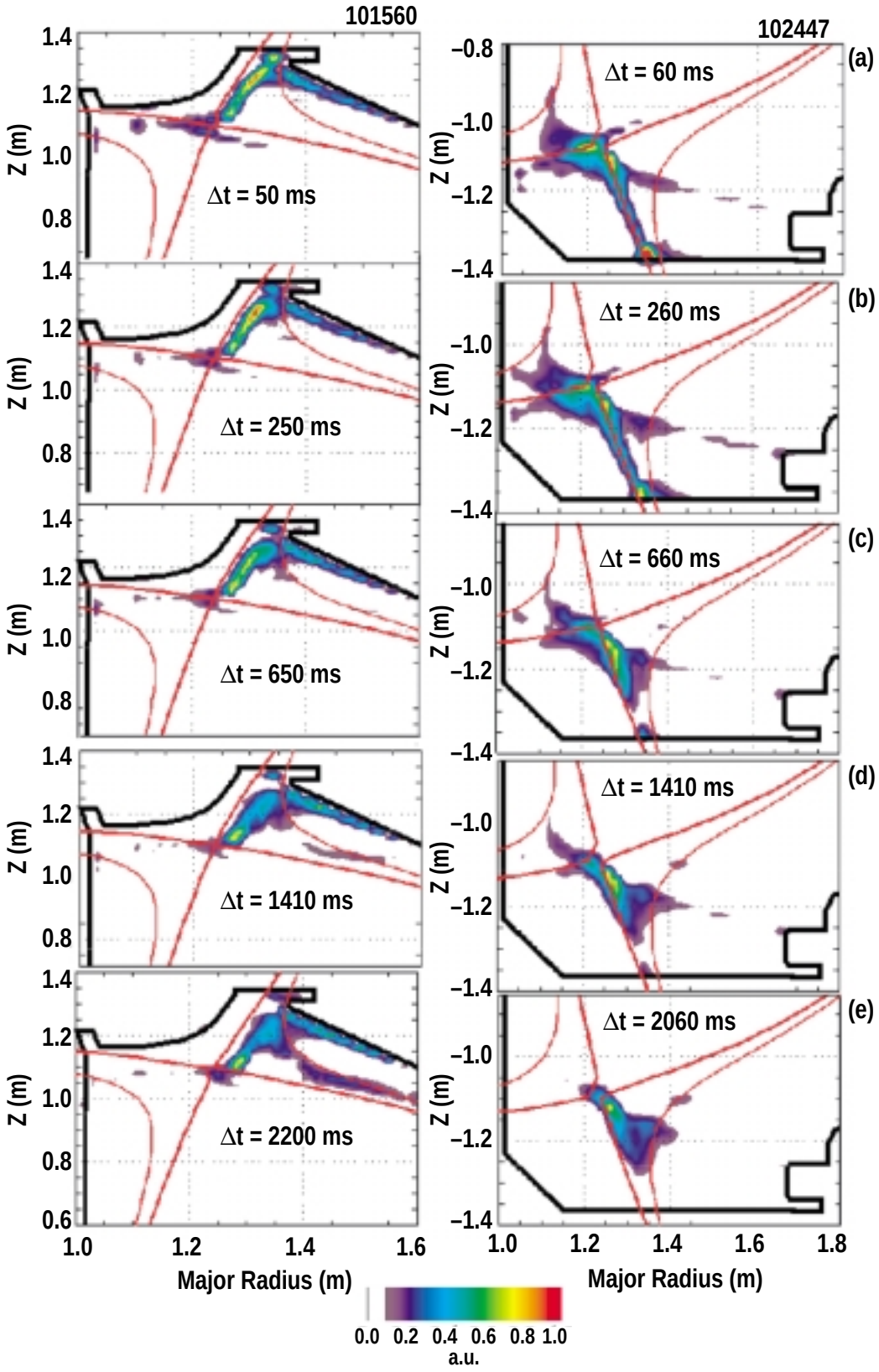

FIG. 5. Evolution of CIII visible emission (465 nm) in the upper (closed) and lower (open) divertors using a high triangularity divertor shape. Elapsed time since gas injection, Δt, is shown. There is evidence (b) of the start of the transition to detachment approximately 250 ms after gas injection. The localized CIII emission in the outer SOL near the X–point (e) that is characteristic of a completed transition to detachment does not occur until approximately 2000 ms later, independent of divertor baffle geometry.

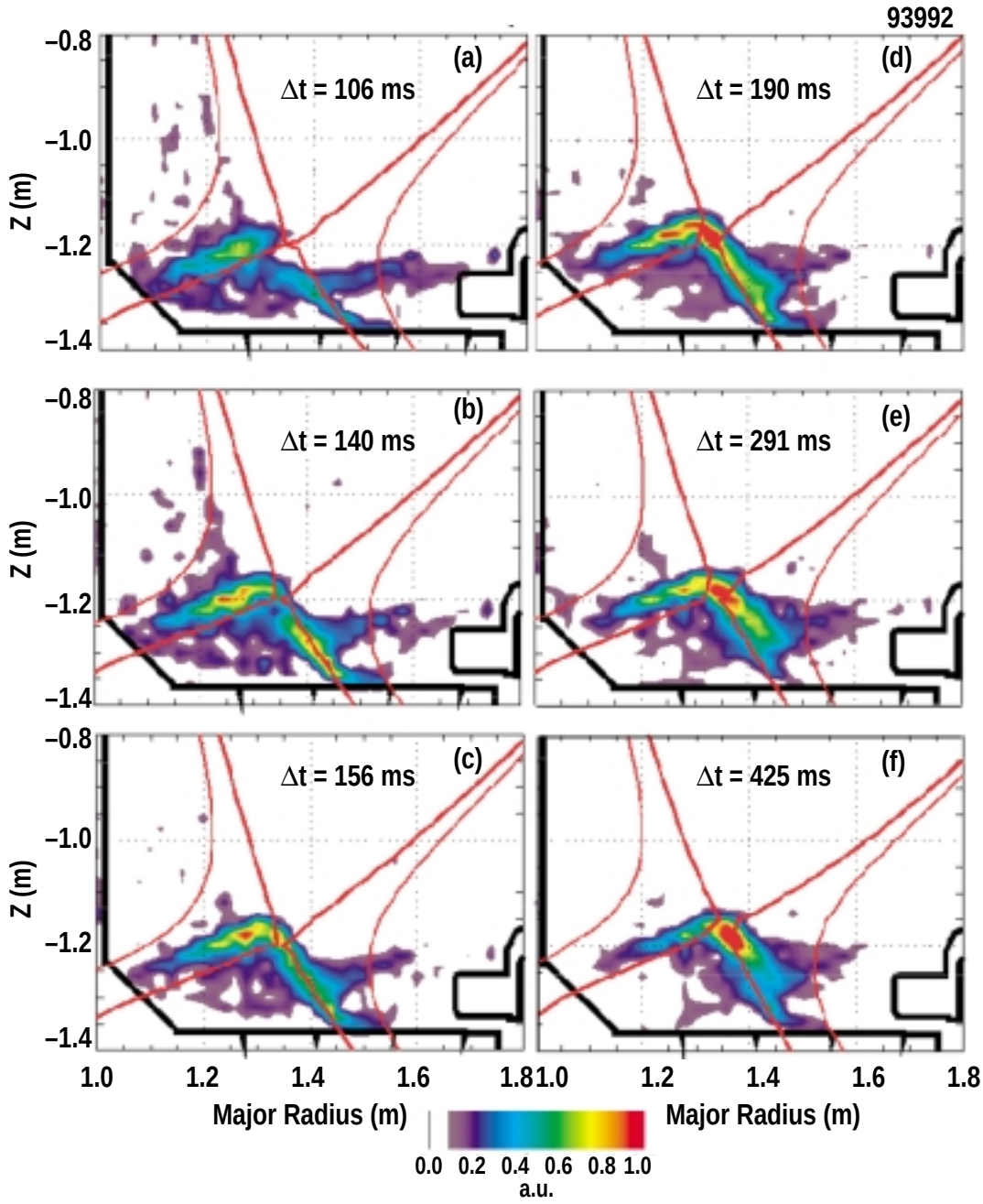

FIG. 6. Evolution of CIII emission from (a) attached, low triangularity ELMing H–mode to (f) detached divertor operation. Elapsed time since gas injection, Δt, is shown. The transition to detachment begins approximately 140 ms after the start of gas injection (b) and is complete within about 300 ms thereafter (f).

4.2. Pumping

The goals of closing the upper divertor with baffling and adding cryopumping were to reduce the flux of recycling neutrals from the divertor back to the core plasma in unpumped operation, to allow low density, $n_e \sim 0.3\ n_{Gr}$, ELMing H–mode operation of high triangularity plasmas by use of divertor pumping, and to provide SOL flow for control of impurities through simultaneous use of gas injection and pumping [30]. The

new upper divertor pumping system pumps both the inner and outer legs of the upper divertor through use of 2 toroidally continuous cryopumps under the private flux and outer baffle structures respectively (Fig. 4). For typical equilibrium configurations the outer pump is in the outer SOL and the inner pump is in the private flux region near the inner strikepoint (Fig. 1). In USN or DN operation the particle exhaust can be controlled by moving the location of the strikepoints with respect to each pump entrance. For nearly DN configurations the particle exhaust can also be controlled with fixed strikepoint position by varying the magnetic balance, dR_{sep}. Since the lower divertor cryopump does not pump at high-δ, shifting dR_{sep} controls the fraction of the scrape-off layer particle flux channeled into the pumped upper divertor.

Detailed strikepoint position sweeps with the ion ∇B drift into the upper divertor showed that the exhaust rate was maximized as the strikepoint was placed close to the pump entrance [11,12]. Detailed strikepoint position sweeps with the ion ∇B drift into the upper divertor showed that the exhaust rate increased as the strikepoint was placed close to the pump entrance [11]. This result was similar to that documented for the outer pump in the open lower divertor at low triangularity [31]. In the outer upper baffle plenum where pressure measurements were available, the plenum pressure, and therefore exhaust rate, was also correlated with strikepoint position. The pumping efficiency, defined as the particle exhaust by the pump normalized to the total plate ion current, $n_{pump} = (2\ P_{baf}\ S_{pump})/(J_{sat}\ R\ dR)$, of the inner upper pump reached ~10% when the inner strikepoint was near the pump entrance [11,12]. The efficiency of the outer pump was somewhat higher. The inner pump efficiency showed a weak maximum when the inner strikepoint was just below the private flux dome baffle [11]. In both cases the exhaust rate appeared to be less sensitive to strikepoint position than the pumping efficiency because changes in strikepoint position from flat target plates to inclined targets changed the total plate ion current [11].

The exhaust rate trends from the strikepoint sweep experiments in attached plasmas are consistent with the baffle design modeling [12] which used a ballistic model [31] of neutral transport near the target plates; detailed comparisons using the experimentally

measured particle flux profiles are in progress [11]. In this model the exhaust rate is expected to be maximized when the fraction of the recycling neutrals that ballistically stream into the pump plenum entrance is maximum. For the outer strikepoint with the pump in the SOL and the ion ∇B drifttoward the X–point, the maximum exhaust rate occurred, as expected, when the strikepoint was as near the entrance as possible without intercepting the peak in the SOL particle flux profile on the outer baffle structure. For the inner pump in the private flux region, the maximum exhaust occurred as expected when the peak in the particle flux profile was as close to the entrance as possible, i.e., where the acceptance cone of ballistic particles that recycle from the inner SOL on the centerpost flat target would be expected to be maximized. Detailed modeling of these effects is in progress [11].

Use of pumping during the L–mode current ramp reduced the wall inventory and the density rise during the ELM-free period after the H–mode transition [11,32]. By pumping with either pump during the current ramp and L–mode phases of the discharge, the walls could be depleted of particles and the core density increase at the H–mode transition was reduced. The time required to reach the desired density, below the natural H–mode density, was reduced when the H–mode transition density rise was reduced. Finally in high density detached plasmas the pumping speed was not as sensitive to strikepoint position as for attached plasmas [10]. This is similar to previous results from the lower, unbaffled divertor at low triangularity [33]. In this case the particle flux on the targets at the strikepoint was substantially reduced and the profile was broader than in attached plasmas so the fraction of the neutrals ballistically entering the pump plenum did not depend strongly on strikepoint position.

Magnetic balance variation studies with the pumps on showed that the outer pump was not as sensitive to dR_{sep} variation as the inner pump [32]. Plasmas were produced initially in DN shape, $dR_{sep} = 0$, with the ion ∇B drift toward the upper divertor, and then the magnetic balance was slowly shifted to an upward unbalanced DN, $dR_{sep} = 1$ cm. For fixed strikepoint positions, the outer baffle plenum pressure remained nearly unchanged during this dR_{sep} variation. However, the inner baffle pressure increased a

factor of 2 as dR_{sep} approached 1 cm. In magnetically balanced DN the inner divertor legs are cutoff from particles that exit the core plasma near the outer midplane and the inner pump pressure is low. As the width of the SOL flux tube that maps to the upper inner divertor increases with dR_{sep} increase, the particle flux to the inner leg increases and the inner pump efficiency increases.

Using these techniques, density control at high triangularity of both L– and H–mode plasmas was achieved [11,34]. Densities as low as 0.3 n/n_{Gr} were achieved in ELMing H–mode. The lower densities allowed experiments to control the core plasma current profile with ECH current drive to begin. Density control is critical in these experiments because for fixed electron pressure the EC current drive efficiency scales at $\eta_{CD} \sim T_e/n_e \sim 1/n_e^2$. These modified current profiles are desired to extend and control the high performance advanced tokamak regime. For a controlled density, long pulse discharge, a record energy input of 50 MJ into the plasma was achieved without increasing the core carbon content [12,34].

5. CONCLUSIONS

The optimization of core and divertor plasma shape and the geometry of divertor baffling involves trade-offs between many competing factors. For attached ELMing H–mode plasmas a high triangularity core plasma produces high normalized energy confinement and beta limit and is therefore desirable for maximization of fusion power density. However, for poloidal field coil designs which must have the PF coils outside the toroidal field coils due to engineering constraints, high triangularity tends to force the plasma configuration close to a double-null shape. The presence of a second X–point inside the vacuum vessel then introduces a whole new set of tradeoffs into the optimization process.

To minimize the peak heat flux to the targets in the divertor regions one might think that the design should be optimized toward a nearly balanced DN in an attempt to share the power losses equally between the two divertors, however this is not the case for several reasons. Asymmetric power and particle losses from the core plasma are

observed with most of the losses coming near the outer midplane, in agreement with theoretical predictions [35]. In this situation if SN and balanced DN plasmas are compared, the power directed along the outer SOL from the midplane toward each of the two divertor legs of the SN is roughly the same as the power directed toward the upper and lower outer legs of the DN. In the balanced DN with the majority of the power lost at the outer midplane the inner legs do not receive much power loading and the core loss power is shared between two divertor legs just as in the SN case.

Considering unbalanced DN shapes the asymmetries of particle drifts determine the optimum magnetic balance for heat and particle flux sharing between the two outer divertor targets. Due to ion ∇B and $E \times B$ drift effects a shape that is magnetically unbalanced slightly away from the ion ∇B drift direction (i.e. with the ion ∇B drift directed out of the primary divertor) is optimum for balancing the peak heat load. However, the peak heat flux balance is very sensitive to the magnetic balance so that if the advantage of heat load sharing is to be achieved then a very sophisticated magnetic balance control system must be included in the design. To further optimize a design with a slightly unbalanced magnetic DN configuration one might try to minimize the volume taken up inside the vacuum vessel by the secondary divertor (i.e., that which receives less of the particle flux and would therefore not have the hardware for active divertor pumping), in an attempt to maximize the core volume for fusion power production. However, as the secondary divertor volume is reduced the high recycling character of this divertor is lost and the secondary divertor plasma becomes sheath limited. This can result in significantly increased sputtering of target surfaces by fast ions accelerated through the sheath in high power scenarios. Finally, with the volume of the secondary fixed above this lower limit one might try to optimize the design of the divertor hardware to take advantage of the asymmetries of heat and particle deposition in the various divertor legs. This would involve placing the highest heat flux capability and the particle pumping system on the outer leg of the primary divertor. In principle the remaining three divertor legs could be designed with reduced heat flux armor and no pumping capability in an optimized design. In addition the volume of the inner SOL and

inner divertor legs could be minimized which optimizes the radial build of the design. However, since the power threshhold for the L-H transition is typically higher for a configuration balanced slightly away from the ion ∇B drift direction, the operating scenario for such a device would then have to include startup scenarios in which the up/down magnetic balance was very well controlled through the L– to H–mode transition. In addition the dR_{sep} balance would need to be controlled very well up to the highest densities of operation because the density at which the plasma falls out of H–mode back to L–mode is significantly lower for magnetic balance shifted away from the ion ∇B drift direction.

Optimized, unbalanced DN operation in ELMing H–mode therefore requires a robust magnetic balance control system capable of precise control of the plasma from startup conditions through the highest H–mode densities. Fortunately the sensitivity of the peak heat flux balance to magnetic balance may provide the "diagnostic" that will enable the control system to perform feedback control of magnetic balance to sufficient accuracy. This would appear to be a key line of research for this route to tokamak optimization.

Finally at high density, when the primary divertor detaches, these studies have shown that the behavior of the plasma as it makes the transition to detachment depends on the shape of the divertor plasma. The detachment evolution is very different in high triangularity divertor shapes compared with low triangularity divertors. However, for our closed divertor baffling configuration with close fitting baffles on the outer leg and private flux region boundaries only, the effect of baffling on detachment evolution was small. Combining these two observations leads to the conclusion that the geometry of the inner divertor leg may play the critical role in the evolution from attached to detached conditions. This might be expected since the inner leg is nearly detached in our low triangularity ELMing H–mode operation at typical H–mode densities even when the outer leg is fully attached. The evolution of the change to detached outer leg operation at low triangularity starts with changes in the radiation profile in the inner leg as gas is injected and the divertor density increases. At high triangularity the changes

leading to detachment in the two divertor legs appear to occur at nearly the same time. Detailed future modeling of detachment scenarios in unbalanced DN shapes that includes E×B and other classical drifts should help to explain these differences [23].

Therefore it appears that there are advantages of unbalanced DN configurations for optimizing tokamak performance. An example of a single point comparison of a SN reference discharge and unbalanced DN shapes with partial optimization in DIII–D using the trends from these studies is given in Ref. [6]. While not exhaustive, this preliminary optimization shows that the unbalanced DN shapes had higher product of normalized pressure and confinement enhancement over L–mode ($\beta_N H_{89ITER}$, where H_{89ITER} is the enhancement over ITER 89 confinement scaling [36]), lower density rise at the L-H transition (advantageous for density control), and lower peak outer leg heat flux. These results indicate that this regime of tokamak plasma shape warrants further study.

ACKNOWLEDGMENT

Work supported by U.S. Department of Energy under Contracts DE-AC03-99ER54463, W-7405-ENG-48, DE-AC004-94AL85000, and DE-AC05-00OR22725.

REFERENCES

[1] ITER Physics Basis Editors, *et al*., Nucl. Fusion, **39**, (1999) 2137.

[2] R.L. Miller, *et al*., Plasma Phys. And Control. Fusion, **40**, 753 (1998).

[3] T.H. Osborne *et al*., J. Nucl. Mater., **266-69**, 131 (1999).

[4] T.W. Petrie *et al.*, Control. Fus. and Plasma. Phys., **23J**, 1237 (1999).

[5] T.H. Osborne *et al.*, Plasma Phys. And Control. Fusion, **42**, 1, (2000).

[6] M.E. Fenstermacher, J. Nucl. Mater., **290-293**, 588-592 (2001).

[7] M.E. Fenstermacher, *et al*., Proc. 18th Int. Conf. on Plasma Physics and Controlled Nuclear Fusion Research, Sorrento, Italy, (2000) IAEA-CN-77/EX2-4, IAEA, Vienna Vol. 1, 609 (2001), also General Atomics Rept. GA-A23504 available at http://fusion.gat.com/pubs-ext/IAEA00/A23504.pdf.

[8] T.W. Petrie, *et al* J. Nucl. Mater., **290-293**, 935-939 (2001).

[9] T.H. Osborne, *et al.,* J. Nucl. Mater., **290-293**, 1013-1017 (2001).

[10] T.W. Petrie, M.E. Fenstermacher, C.J. Lasnier, Fusion Technology, **39** (2001) 916.

[11] J.G. Watkins, *et al*., "Pumping Efficiency and Particle Control in DIII–D," Bull. Am. Phys. Soc., Vol. 45, available at http://fusion.gat.com/pubs-ext/APS00/Watkins pos.pdf, to be submitted for publication in Nucl. Fusion.

[12] M.A. Mahdavi, *et al*., J. Nucl. Mater., **290-293**, 905-909 (2001).

[13] T.W. Petrie, *et al*., "Effects of Open and Closed Divertor Geometries on Plasma Behavior in DIII–D," Proc. 28th European Physical Society Conf. On Controlled Fusion and Plasma Physics, Madiera, Portugal, (2001).

[14] A. Loarte, Plas. Phys. Control. Fusion, **43** (2001) R183-224.

[15] H. Zohm, *et al.,* Plasma Phys. And Control. Fusion, **38**, (1996) 1497.

[16] E.A. Lazarus, *et al*., Proc. 15th Int. Conf. on Plasma Physics and Controlled Nuclear Fusion Research, Seville, Spain, (1994) IAEA-CN-60/A5-1, IAEA, Vienna Vol. 1, 609 (1995)

[17] G.L. Jackson, *et al*., Phys. Rev. Lett. **67** (1991) 3098.

[18] M. Greenwald, *et al.,* Nucl. Fusion **28** (1988) 2199.

[19] A.W. Leonard, A. Herrmann, *et al.,* J. Nucl. Mater., **266-269**, 109-113 (1999).

[20] A.W. Leonard, *et al.,* J. Nucl. Mater., **290-293**, 1097-1101 (2001).

[21] A.V. Chankin *et al.,* J. Nucl. Mater., **241-243**, (1997) 199, and A.V. Chankin *et al.*, J. Nucl. Mater., **290-293**, (2001) 518.

[22] T.W. Petrie *et al.,* J. Nucl. Mater., **266-269**, (1999) 642.

[23] M.E. Rensink, S.L. Allen, G.D. Porter, T.D. Rognlien, Contrib. Plasma Phys. **40** (2000) 302., and M.E. Rensink, *et al.,* J. Nucl. Mater. **290-293** (2001) 706.

[24] C.J. Lasnier, *et al* J. Nucl. Mater., **290-293**, 1093-1096 (2001).

[25] T.W. Petrie, private communication.

[26] N.S. Wolf *et al.*, Bull. Am. Phys. Soc., **45** (2000) 154, available at http://fusion.gat.com/pubs-ext/APS00/Wolf_vgs.pdf.

[27] T.W. Petrie *et al.*, Nucl. Fusion, **37** (1997) 643.

[28] M.E. Fenstermacher *et al.*, Phys. Plasmas, **4**, (1997) 1761.

[29] M.E. Fenstermacher *et al.*, J. Nucl. Mater., **266-269** (1999) 348.

[30] S.L. Allen *et al.*, Nucl. Fusion, **39** (1999) 2015.

[31] R. Maingi *et al*., Nucl. Fusion, **39** (1999) 1187.

[32] M.R. Wade, private communication, available at http://fusion.gat.com/pubs-int/Presentations/YrEndRev01/Wade.pdf.

[33] T.W. Petrie *et al.*, Nucl. Fusion, **37** (1997) 321.

[34] S.L. Allen *et al*., J. Nucl. Mater., **290-293** (2001) 995.

[35] X.Q. Xu *et al.*, Proc. 13th U.S. Transport Taskforce Workshop (2000) to be published.

[36] ITER Physics Basis Editors *et al*., Nucl. Fusion, **39** (1999) 2137.